Mem. S.A.It. Vol. 91, 241

Memorie della

Three-dimensional hydrodynamical simulations of supernova explosions in the smallest Milky Way satellites

Donatella Romano[1], F. Calura[1], G. C. Few[2], and A. D'Ercole[1]

[1] Istituto Nazionale di Astrofisica – Osservatorio di Astrofisica e Scienza dello Spazio di Bologna, via Gobetti 93/3 40129 Bologna, Italy, e-mail: donatella.romano@inaf.it
[2] E.A. Milne Centre for Astrophysics, University of Hull, Cottingham Road, Kingston Upon Hull HU6 7RX, UK

Abstract. In the past fifteen years, a new class of galaxy has been discovered that is made of faint, old, scarcely evolved stellar systems –the so-called ultrafaint dwarf galaxies (UFDs). High-resolution, three dimensional hydrodynamical simulations are a powerful tool to investigate the nature, origin, and evolution of UFDs, but they are extremely expensive in terms of computational time. We took advantage of high performance computing (HPC) resources provided by CINECA through the MoU INAF-CINECA and started a project devoted to the study of UFDs. Preliminary results of our ongoing project are discussed in this contribution.

1. Introduction

In the ΛCDM concordance cosmology, large halos form from the merging and accretion of smaller building blocks (White & Rees 1978); however, a large number of sub-halos is predicted to survive the digestion processes and inhabit the main galaxy halo. In the past fifteen years, the number of known Milky Way (MW) companions has increased apace, thanks to the commitment of hundreds of scientists around the world to deep large-area sky imaging surveys. A new class of galaxy has been discovered, one made of extremely faint, dark-matter dominated, scarcely evolved stellar systems, that have been given the name of ultrafaint dwarf galaxies (UFDs; Willman et al. 2005). All of this has dramatically impacted our understanding of the way the halo of our Galaxy came into being. The continuing discovery of more and more UFDs, even at the detectability limits of the surveys (see Torrealba et al. 2016, their figure 9), pulls the trigger on studies aimed at establishing how star formation and chemical enrichment proceed in small dark matter halos.

Semi-analytical and pure chemical evolution models rely on simple, yet physically motivated, parameterizations and heuristic prescriptions to trace the evolution of several chemical elements in the interstellar medium (ISM) of systems with structural properties similar to those of observed UFDs. They generally agree that these galaxies formed stars very inefficiently, converting into stars less than 1-3 per cent of their baryons, but there is no consensus about the mechanism(s) that truncate(s) the star formation, with either reionization, galactic winds or tidal stripping being suggested (Salvadori & Ferrara 2009; Vincenzo et al. 2014; Romano et al. 2015).

Chemical evolution models have been very successful in explaining many observed properties of galaxies but, when moving to stellar systems with lower and lower dynamical masses, the parameterizations adopted to treat the thermal feedback from stars, the conditions imposed on the onset of galactic-scale outflows, the assumed mass loading factors for the neutral ISM, all introduce degeneracies in the proposed solutions. Furthermore, there are severe limitations in the treatment of spatial inhomogeneities. That is why chemical evolution models can not put firm constraints to the physical processes regulating the evolution of the lowest mass systems (see, e.g., the discussion in Romano et al. 2015). The natural outcome is to turn to hydrodynamical simulations.

2. Numerical setup

We used a customized version of the Adaptive Mesh Refinement (AMR) code RAMSES (Teyssier 2002) to investigate the fate of the gas following multiple supernova (SN) explosions in a prototype UFD. The initial configuration is designed to mimic a well-studied system, the Boötes I UFD (see Romano et al. 2015, and references therein), and foresees a non-rotating distribution of gas and stars embedded in an isolated dark matter halo.

The initial baryonic and dark masses are $M_{gas} = 6{\times}10^6 M_\odot$ and $M_{DM} = 3.5{\times}10^7 M_\odot$ and follow, respectively, a Plummer (1911) density profile, with a characteristic radius of 200 pc, and a Burkert's (1995) profile, with cut-off radius of 1.2 kpc. The dark matter component is modeled as a static external potential and added to the solution of the Poisson equation; the self-gravity of the gas is neglected for simplicity. The initial pressure profile is set by solving the hydrostatic equilibrium equation.

A population of coeval stars, $M_{stars} = 10^5 M_\odot$, is set in place at the beginning of the simulation. Assuming a Kroupa (2001) stellar initial mass function, 650 of these stars are assigned initial masses in excess of 8 $M_\odot$. The massive stars are grouped in ten OB associations 8 pc wide scattered across the computational volume, following the procedure outlined in Calura et al. (2015). Each association is allowed to inject mass and energy in its surroundings at a constant rate for an uninterrupted period of 30 Myr (roughly corresponding to the lifetime of a 8 $M_\odot$ star) through both stellar winds and SN explosions (cf. Mac Low & McCray 1988). The mass and energy injection rates during the pre-SN phase (lasting 3 Myr) and SN phase (from 3 to 30 Myr) for each OB association are computed after Leitherer et al. (2014). Mass and energy are spread on the volume occupied by the OB association.

The computational box is L = 2 kpc on a side, with a maximum refinement level corresponding to a minimum cell size of Δx_{min} = 0.95 pc. The refinement strategy is geometry and discontinuity-based. In particular, at each time step a number of cells at the highest refinement level is set up to cover the regions occupied by the OB associations. This assures that every OB association is adequately spatially resolved: stellar ejecta and SN energy are added to the gas within a sphere that is four grid cells in radius, which prevents the occurrence of square-shaped shock fronts. We use free outflow boundary conditions and create a passive scalar to trace the evolution of the metallicity of the gas in each cell, starting from a primordial (zero) metallicity value. To minimize numerical problems, we set a temperature floor of T_{min} = 3900 K. In the following, we present preliminary results for our fiducial high-resolution adiabatic and cooling models.

3. Preliminary results

At the beginning of the simulation, because of the relatively low densities ($n_H \sim 7$ cm^{-3} at the centre and ~ 1 cm^{-3} at the Plummer radius) the radiative cooling is fairly ineffective. Large cavities filled with tenuous hot gas are carved out around the OB associations already during the pre-SN phase (0–3 Myr), *both in the adiabatic run and in the simulation with radiative cooling* (Fig. 1, upper panels), without any need for switching off cooling artificially. During the SN phase (3–30 Myr; Fig. 1, middle and lower panels; shown here is only the behavior up to 13 Myr), in the presence of radiative cooling multiple SN explosions dig superbubbles smaller than those moulded in the

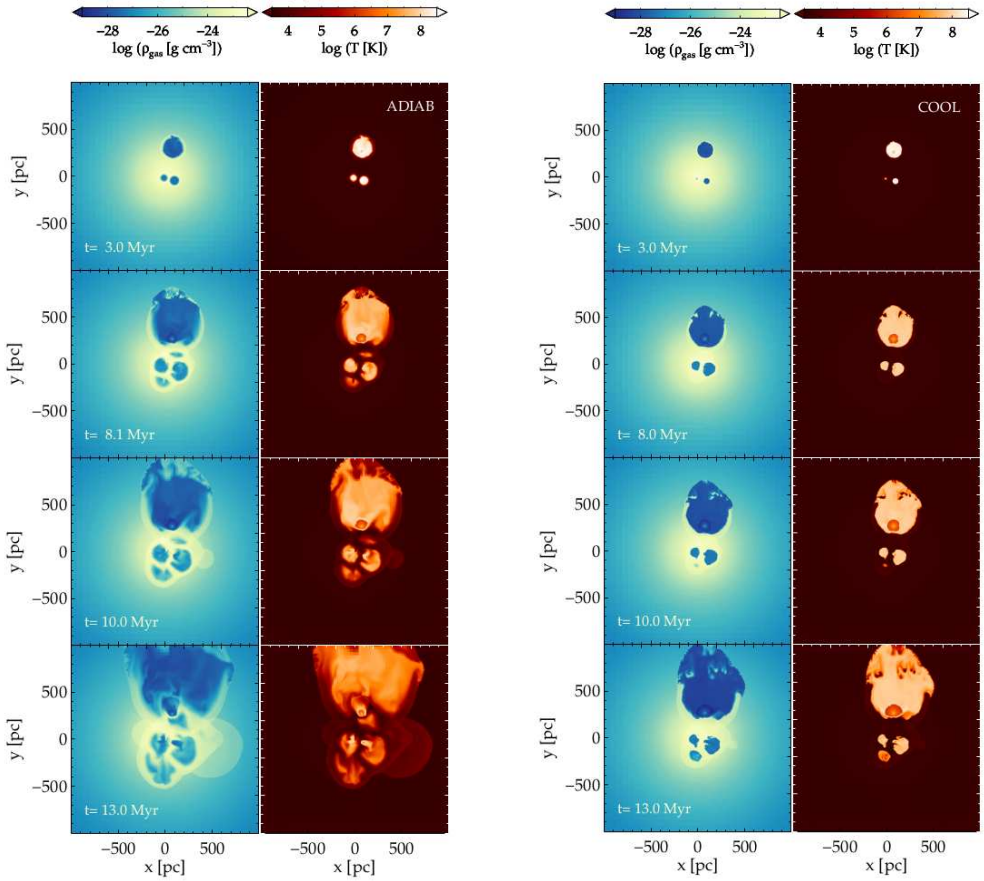

Fig. 1. Gas density and temperature maps in the $z = 0$ plane for our fiducial adiabatic (left-hand panels) and radiative (right-hand panels) simulations at different times.

adiabatic case, filled with hotter and more rarefied gas. These bubbles also take more time to lose their individuality, disrupt, and merge. We note that, in spite of the growth of Rayleigh-Taylor instabilities at the borders, the bubbles preserve ovoid shapes delimited by thin, dense, cold shells, until they do not interact with each other. Fig. 3 depicts the gas velocity field at the end of the adiabatic simulation. Pockets of tenuous, heated gas around individual OB associations expand at supersonic velocity. SN debris are channeled in hot structures, that resemble chimneys and fountains, and can either be entrained in an outflow or rain back to the galaxy centre with velocities up to several hundreds of km s^{-1} . The cooler ambient medium is largely unaffected by the SN activity and likely to remain bound; however, a part of it (mostly in the outermost regions) is swept up and steadily moves outwards with velocities that exceed the local escape velocity (see inset in Fig. 3, where the black areas highlight regions where the velocity is lower than the escape velocity from the system). In the adiabatic run most of the mass and energy injected by massive stars in the ISM escape the system. The evolution of the gas density profile is shown in Fig. 4. For the simulation with cooling, the profile at $t = 18$ Myr (green solid curve) differs only slightly form the initial one (black solid curve), which means that, to a large extent, the ambient medium is basically unaffected by the mass

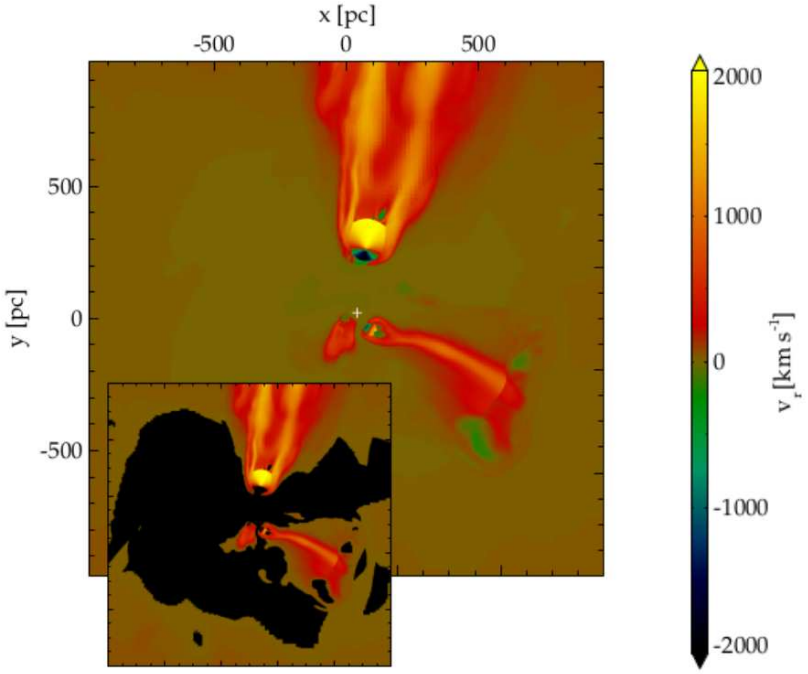

Fig. 2. Gas radial velocity field at the end of the adiabatic simulation in the $z = 0$ plane.

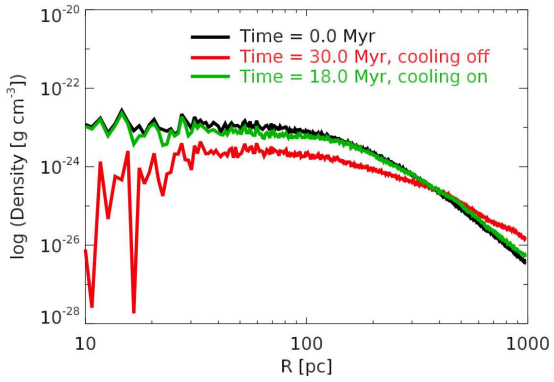

Fig. 3. Gas density profile for the adiabatic (red curve) and radiative (green curve) simulations at different times. The initial profile is shown as the solid black line.

return from SNe. On the other hand, the final profile (at $t = 30$ Myr) for the adiabatic simulation (red solid curve) deviates appreciably from the initial one: it is shallower, with densities two order of magnitudes lower at the centre and slightly higher at radii beyond 400 pc.

Note. The results of the full set of simulations are discussed in Romano et al. (2019), to which we address the interested reader.

Acknowledgements. We acknowledge the computing centre of Cineca and INAF, under the coordination of the "Accordo Quadro MoU per lo svolgimento di attività congiunta di ricerca Nuove frontiere in Astrofisica: HPC e Data Exploration di nuova generazione", for the availability of computing resources and support.

References

Burkert, A. 1995, ApJ, 447, L25
Calura, F., et al. 2015, ApJ, 814, L14
Kroupa, P. 2001, MNRAS, 322, 231
Leitherer, C., Ekström, S., Meynet, G., et al. 2014, ApJS, 212, 14
Mac Low, M.-M., McCray, R. 1988, ApJ, 324, 776
Plummer, H. C. 1911, MNRAS, 71, 460
Romano, D., et al. 2015, MNRAS, 446, 4220
Romano, D., et al. 2019, A&A, 630, A140
Salvadori, S., Ferrara, A. 2009, MNRAS, 395, L6
Teyssier, R. 2002, A&A, 385, 337
Torrealba, G., Koposov, S. E., Belokurov, V., et al. 2016, MNRAS, 463, 712
Vincenzo, F., et al. 2014, MNRAS, 441, 2815
White, S. D. M., Rees, M. J. 1978, MNRAS, 183, 341
Willman, B., Blanton, M. R., West, A. A., et al. 2005, AJ, 129, 2692